PAPER

Graphitic carbon nitride nanosheet supported silica nanochannel film for enhanced electrochemiluminescence sensing of 2,4,6-trichlorophenol and prochloraz†

Junqi Feng,‡[a] Yanyan Zheng,‡[b] Tao Luo,[a] Fengna Xi ⓘ *[b] and Hao Lai*[a]

The development of simple, rapid, and sensitive methods for detecting pesticide in environmental and food samples holds significant importance. Electrochemiluminescence (ECL) sensing platforms with high resistance to interference and contamination, and reduced consumption of ECL emitters, are highly desirable for such applications. In this work, we present an ECL sensing platform based on a graphitic carbon nitride nanosheets (CNNS) supported vertically ordered mesoporous silica film (VMSF) modified glassy carbon electrode (GCE) for the highly sensitive detection of the environmental pollutant 2,4,6-trichlorophenol (TCP) and the broad-spectrum insecticide prochloraz. Two-dimensional (2D) CNNS were synthesized by exfoliating bulk graphitic carbon nitride (g-C_3N_4) using concentrated sulfuric acid, serving as a novel conductive and adhesive layer for the growth of a stable VMSF on GCE *via* an electrochemical assistance self-assembly (EASA) method to prepare VMSF/CNNS/GCE. The electrostatic enrichment capability of VMSF nanochannels for the positively charged ECL emitter tris(2,2′-bipyridyl) ruthenium(II) ($Ru(bpy)_3^{2+}$) realized stable and significantly enhanced ECL signals at a low concentration of $Ru(bpy)_3^{2+}$ (10 μM). Based on the quenching effect of TCP on the ECL signal of $Ru(bpy)_3^{2+}$, highly sensitive ECL detection of TCP was achieved by the VMSF/CNNS/GCE with a linear range from 10 nM to 0.7 mM and a low detection limit (DL) of 2.2 nM. As the metabolic end product of prochloraz is TCP, indirect ECL detection of prochloraz was also accomplished by measuring the produced TCP. Combined with anti-fouling and anti-interference abilities, as well as signal amplification of VMSF, the developed VMSF/CNNS/GCE sensor enabled the sensitive ECL detection of TCP in pond water and prochloraz in orange peel extract.

1. Introduction

Widespread pesticide use has led to an increasingly severe issue of pesticide residue contamination in food and the environment. Prochloraz (*N*-propyl-*N*-[2-(2,4,6-trichlorophenoxy)ethyl]-1*H*-imidazole-1-carboxamide) is an efficient imidazole-type broad-spectrum fungicide that inhibits the synthesis of ergosterol, disrupts fungal cell membranes, and achieves fungicidal effects.[1,2] Currently, prochloraz is widely employed in agriculture, such as in the treatment and eradication of crop diseases caused by pathogens like *Fusarium* and *Phytophthora*.[3,4] However, prochloraz exhibits strong biological toxicity, causing skin irritation and significant disruption to the endocrine levels

of mammals. Additionally, the metabolic degradation product of prochloraz is 2,4,6-trichlorophenol (TCP), which possesses notable pathological and toxicological effects, along with potential carcinogenicity.[5,6] Thus, developing simple, rapid, and sensitive method for detecting prochloraz and TCP in environmental and food samples holds significant importance. Traditionally, high-performance liquid chromatography (HPLC) and gas chromatography coupled with mass spectrometry (GC-MS) have been employed for trace detection of TCP.[7] Although these methods offer high reproducibility and low detection limits, they require substantial extraction of environmental water with complex purification steps. Additionally, the equipment is expensive, and the procedures are cumbersome, demanding skilled operators, which poses challenges to the detection process. Therefore, it is crucial to develop a simple, fast, and sensitive analytical method to detect TCP in environmental samples for human health and environmental protection.

Electrochemiluminescence (ECL) is a chemical luminescence induced and controlled by electrochemical reaction.[8–10]

[a]Guangxi Medical University Cancer Hospital, Guangxi Medical University, Nanning 530021, China. E-mail: laihao@gxmu.edu.cn

[b]School of Chemistry and Chemical Engineering, Zhejiang Sci-Tech University, Hangzhou 310018, China. E-mail: Fengnaxi@zstu.edu.cn

‡ The two authors contributed equally.

Typically, substances on the electrode surface generate excited states through high-energy electron transfer, and the transition of the excited state back to the ground state produces luminescence. ECL encompasses both electrochemical reactions occurring on the electrode surface and chemiluminescent reactions among electroactive species.[11–13] Thus, ECL combines the advantages of traditional chemiluminescence, such as high sensitivity and a wide linear range, with the benefits of electrochemical analysis equipment, convenient operation, rapid analysis, and strong controllability.[14–18] However, when detecting complex environmental samples, matrix effect may cause significant interference with experimental results, thereby reducing the sensitivity and accuracy of ECL detection. Furthermore, in the process of ECL analysis, a significant amount of emitters is consumed. Common ECL emitter, such as complex of ruthenium bipyridine, is relatively costly. Although there have been studies proposing the immobilization of ECL reagents on the electrode surface, this approach may compromise detection sensitivity and stability. Therefore, enhancing the electrode's resistance to interference and contamination, along with reducing the consumption of ECL emitter, is crucial for ECL detection of complex samples.

Using porous materials to modify electrodes is an effective strategy to enhance electrode performance.[19–21] Porous materials exhibit various unique advantages, including high surface area, well-defined pore structures, and controllable pore size and volume, making them highly advantageous in fields such as adsorption, catalysis, and sensing.[22–25] Over the past few decades, mesoporous silica materials have been one of the most significant porous materials. In comparison to mesoporous nanoparticles, vertically ordered mesoporous silica film (VMSF) represents a class of highly ordered porous membrane materials with nanochannels perpendicular to the electrode substrate.[26] On one hand, the ultra-small nanochannels (typically 2–3 nm) exhibit size exclusion effects, allowing VMSF nanochannels to resist the entry of large molecules such as cells, proteins, and DNA.[27,28] Combining this with the insulating structure of silica, VMSF-modified electrodes can effectively exclude interference from large molecules or particles in complex sample matrices. On the other hand, VMSF nanochannels provide charge-selective permeability.[29] As silanol groups on VMSF have low pK_a (around 2–3), they can be deprotonated at commonly medium, leading to a negatively charged surface.[30] Consequently, VMSF can exclude negatively charged small molecules while adsorbing positively charged ones.[31–34] For instance, VMSF exhibits significant electrostatic adsorption towards the positively charged ECL emitters, tris(2,2′-bipyridyl)ruthenium(II) (Ru(bpy)$_3$$^{2+}$), leading to significant enhancement of the ECL signal.[35] This signal amplification effect allows for highly sensitive ECL detection at low concentrations of Ru(bpy)$_3$$^{2+}$, effectively reducing the consumption of ECL reagents and lowering the analytical cost. Additionally, common electrochemical small molecules in biological and environmental samples, such as uric acid (UA) and ascorbic acid (AA), are charge-excluded by VMSF nanochannels.[29] Therefore, VMSF-modified electrodes hold enormous potential

for complex sample detection and can significantly reduce the usage of ECL emitters.

In current research based on VMSF, commonly used supporting electrodes include indium tin oxide electrodes (ITO),[36–40] glassy carbon electrodes (GCE),[41,42] and gold electrodes (AuE).[43,44] VMSF is stably modified on the surface of ITO through O–Si–O covalent bonds, but the ECL activity of Ru(bpy)$_3$$^{2+}$ on ITO is very low. For carbon-based electrodes or metal electrodes, sufficient adhesion layer or pre-treatment is required to increase the surface oxygen-containing functional groups of the electrode, allowing VMSF to adhere persistently to the electrode substrate. Researchers have employed organosilane modification on the electrode as an adhesive to improve the stability of VMSF on the electrode.[29] However, this non-conductive adhesive layer can passivate the electrochemical activity of the electrode, reducing detection sensitivity. Our research group employed reduced graphene oxide (rGO) as the adhesive layer, successfully growing VMSF on carbon electrode,[45–47] and achieving highly sensitive detection of drug molecules and biomarkers. We also found that electrochemical polarization pretreatment of GCE (p-GCE) can generate abundant oxygen-containing functional groups on the electrode surface. Without the need for any adhesive, VMSF can be directly integrated on p-GCE while maintaining excellent adhesion and chemical stability.[48,49] However, the oxygen-containing functional groups in rGO or p-GCE, such as phenolic hydroxyl groups, can oxidize to quinone-like substances during electrode scanning.[50] This oxidation leads to significant resonance energy transfer between quinone-like substances and Ru(bpy)$_3$$^{2+}$, thereby reducing the ECL signal and lowering detection sensitivity.[51] Therefore, the development of novel adhesive layers holds great potential for expanding the application of VMSF in ECL analysis.

In this work, graphitic carbon nitride nanosheet (CNNS) was utilized for the first time as both the adhesive and electroactive layer, successfully achieving stable modification of VMSF on glassy carbon electrode. As a 2D material with large surface area and excellent biocompatibility, CNNS is characterized by the sp^2 hybridization of C and N elements, forming chemical bonds and creating a highly delocalized π-conjugated system resembling a benzene ring.[52–54] Consequently, CNNS exhibits good conductivity, and its two-dimensional structure facilitates the formation of a smooth electrode modification layer. On the other hand, after acid treatment, CNNS surface generates oxygen-containing functional groups, such as hydroxyl groups. This not only contributes to the stable binding of VMSF but also does not lead to a significant quenching effect on the ECL signal of Ru(bpy)$_3$$^{2+}$ as these functional groups have weak electrochemical activity. After modifying CNNS on the GCE surface (CNNS/GCE), VMSF was rapidly and stably grown using an electrochemical-assisted self-assembly method (EASA) to form VMSF/CNNS/GCE. Combining the electrostatic adsorption capacity of VMSF nanochannels for Ru(bpy)$_3$$^{2+}$, the ECL signal on VMSF/CNNS/GCE was significantly enhanced. Taking into account the quenching effect of TCP on the ECL signal of Ru(bpy)$_3$$^{2+}$, VMSF/CNNS/GCE achieved direct and highly sensitive detection of TCP. As TCP is the metabolic degradation

product of prochloraz, indirect ECL detection of prochloraz in fruits was achieved.

2. Experimental

2.1 Materials and reagents

Hexadecyltrimethylammonium bromide (CTAB, 99%), tetraethyl orthosilicate (TEOS, 98%), potassium hexacyanoferrate(III) ($K_3[Fe(CN)_6]$, 99.5%), potassium hexacyanoferrate(II) trihydrate ($K_4[Fe(CN)_6]\cdot 3H_2O$, 99.5%), tris(2,2′-bipyridyl) dichlororuthenium(II) hexahydrate ($Ru(bpy)_3Cl_2\cdot 6H_2O$), triethylamine (Et_3N), 1,3,6-trichlorobenzene (TCP), and prochloraz were purchased from Aladdin Technology Co., Ltd. (Shanghai, China). Acetone, anhydrous ethanol, and concentrated sulfuric acid (H_2SO_4) were obtained from Gaojing Fine Chemical Co., Ltd. (Hangzhou, China), while hydrochloric acid (HCl) was acquired from Shuanglin Chemical Reagent Co., Ltd. (Hangzhou, China). Melamine was obtained from Yonghua Fine Chemical Co., Ltd. (Nanjing, China). Phosphate buffer solution was prepared by mixing Na_2HPO_4 and NaH_2PO_4 in certain proportions. Oranges were purchased from a local supermarket (Hangzhou, China), and pond water was collected from the pond at Zhejiang Sci-Tech University (Hangzhou, China). All reagents used were of analytical grade and were not further processed. Ultra-pure water (18.0 MΩ cm) was used throughout the experimental procedures.

2.2 Characterizations and instrumentations

Morphology of VMSF was characterized using transmission electron microscopy (TEM, HT7700, Hitachi, Japan) operated at an accelerating voltage of 100 kV. To prepare TEM sample, VMSF was scraped from GCE surface using a knife, which was dispersed in ethanol by ultrasonication. The resulting dispersion was dropped onto a copper grid, dried under an infrared lamp, and then observed by TEM. Electrochemical impedance spectroscopy (EIS) and cyclic voltammetry (CV) tests were conducted on an Autolab (PGSTAT302N) electrochemical workstation (Metrohm, Switzerland). Electrochemiluminescence (ECL) measurement was carried out using an MPI-E II instrument (Xi'an Ruimai Analytical Instrument Co., Ltd.). Both electrochemical and ECL tests were performed in a conventional three-electrode system at room temperature. Specifically, Ag/AgCl served as the reference electrode, platinum wire electrode act as the counter electrode, bare or modified GCE was as the working electrode. Fourier-transform infrared spectroscopy (FTIR) characterization was conducted with a potassium bromide pellet (Nicolet Avatar 370, Thermo, USA).

2.3 Preparation of CNNS

Bulk graphitic carbon nitride (g-C_3N_4) was obtained by thermal condensation of melamine.[53] Briefly, 5 g of melamine was placed in a crucible and heated in an air atmosphere at a rate of 6 °C per minute to 520 °C, and then calcined at this temperature for 4 hours. The resulting yellow solid powder was ground. To prepare CNNS, 2 g of g-C_3N_4 was mixed with 40 mL of concentrated sulfuric acid (98 wt%) and stirred at room temperature for 10 hours.[53] The mixture was poured into ultrapure water and sonicated for 8 hours. The obtained precipitate was repeatedly washed with ultrapure water at 12 000 rpm to obtain a stable CNNS colloid solution. Finally, the CNNS powder was obtained by freeze-drying treatment.

2.4 Fabrication of VMSF/CNNS/GCE

Glassy carbon electrode (GCE, with a diameter of 3 mm) was polished successively with 0.3 μM and 0.05 μM aluminium oxide (Al_2O_3) slurry. After rinsed with ultrapure water, it was sonicated in ultrapure water for 60 s to remove surface residues and dried with nitrogen. The polished GCE exhibited a glossy mirror-like surface under natural light. Then, 10 μL of CNNS colloid was dropped onto the polished GCE electrode and dried at 60 °C, leading to CNNS/GCE electrode. Then, VMSF was grown using the EASA method.[55] Specifically, the precursor solution for VMSF growth was prepared by stirring 1.585 g CTAB and 2.833 g TEOS in a mixture of 20 mL ethanol and 20 mL $NaNO_3$ (0.1 M, pH 2.6) for 2.5 h. Then, the three-electrode system was used with CNNS/GCE as the working electrode. A constant voltage of −2.2 V was applied on CNNS/GCE for electrodeposition for 5 s. After the deposition, the electrode was quickly removed, rinsed with a large amount of ultrapure water and aged at 80 °C overnight. In the resultant electrode, surfactant micelles (SM) were initially present in the nanochannels, denoted as SM@VMSF/CNNS/GCE. Subsequently, the SM was eliminated by immersing the SM@VMSF/CNNS/GCE in an HCl solution (0.1 M in ethanol) for 5 minutes. The resulting electrode was then labelled as VMSF/CNNS/GCE.

2.5 ECL detection of TCP and prochloraz

PBS (0.01 M, pH 7) containing $Ru(bpy)_3^{2+}$ (10 μM) and Et_3N (15 mM) was used as the electrolyte for detecting prochloraz and TCP. To detect TCP, ECL signals were recorded on VMSF/CNNS/GCE in the presence of varying concentrations of TCP. Prochloraz was indirectly detected after undergoing hydrolysis with hydrochloric pyridine salt to produce TCP. For real sample analysis, pond water was initially filtered using a 0.22 μm nylon filter film and then diluted by a factor of 50 using the electrolyte. Orange peel was prepared using a diagonal cutting method, and a quartering technique was employed for sampling. The samples were then pretreated following the procedure outlined in NY/T 1456-2007 (China). Finally, prochloraz and hydrochloric acid pyridine salt were added to the extract. Two millilitres of the extract were mixed with 5 g of pyridine hydrochloride for prochloraz hydrolysis. After the pyridine hydrochloride salt dissolved to hydrolyse prochloraz. The temperature was raised to 210–240 °C after the pyridine hydrochloride salt dissolved, and the mixture was refluxed for 1 h to obtain the TCP hydrolysis solution.

3. Results and discussion

3.1 Stable modification of GCE by VMSF using CNNS as the binding and electroactive layer

As illustrated in Fig. 1, CNNS was applied for the first time as the binding layer and electroactive layer, leading to the
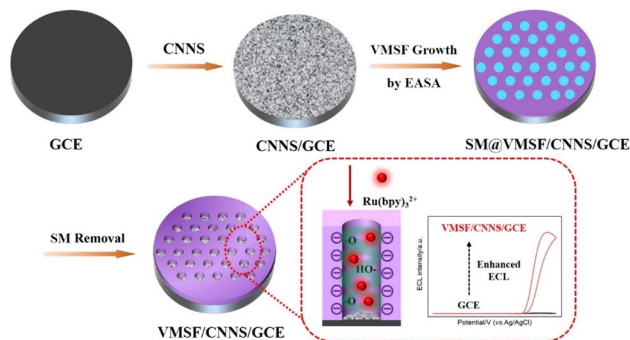
Fig. 1 Illustration for the preparation of VMSF/CNNS/GCE and the improved ECL signals through electrostatic attraction of Ru(bpy)$_3^{2+}$ through VMSF nanochannels.

successful and stable modification of GCE by VMSF. CNNS, a 2D nanomaterial with numerous advantages, combines the exceptional properties of graphene and nitrogen-doped carbon, showing unique physical and chemical characteristics. For instance, the C and N elements in its structure form chemical bonds in a sp^2 hybridized manner, alternating to create a highly delocalized π-conjugated system resembling a benzene ring structure. Consequently, CNNS exhibits excellent conductivity. Furthermore, CNNS displays outstanding mechanical strength and flexibility, and its 2D sheet structure facilitates the formation of a modification layer on the GCE surface through π–π interactions. CNNS can be obtained by exfoliating bulk graphitic carbon nitride (g-C$_3$N$_4$) in an acidic solution. The obtained CNNS surface generates oxygen-containing functional groups such as hydroxyl groups, which contribute to stable binding with VMSF. Simultaneously, the weak electrochemical activity of hydroxyl groups, which ensures no interference with the ECL signal of Ru(bpy)$_3^{2+}$. Therefore, serving as the binding layer and electroactive layer, CNNS successfully achieves stable modification of GCE by VMSF.

Subsequently, VMSF was grown on CNNS/GCE using the electrochemical assistance self-assembly method (EASA). EASA is a technique for rapidly growing VMSF at room temperature. In this method, a suitable negative potential or negative current is applied to the electrode immersed in an acidic precursor solution containing siloxane reagent and a cationic surfactant (cetyltrimethylammonium bromide, CTAB). The electrode surface undergoes a cathodic reduction of H$_2$O, generating a large amount of OH$^-$ and a local increase in pH. This triggers the assembly of cationic surfactants on the electrode surface and the sol–gel reaction of siloxanes, ultimately resulting in VMSF containing the CTAB template (SM@VMSF/CNNS/GCE). After removing the micelles, an electrode with an array of open nanochannels is obtained (VMSF/CNNS/GCE).

The ultrasmall nanochannel and abundant silanol groups of VMSF impart it with charge-selective permeability. As silanol group has the pK_a of approximately 2–3, it ionizes in commonly used media, generating a negatively charged surface that facilitates the transport of positively charged substances. Consequently, the negatively charged nanochannels exhibit a pronounced electrostatic attraction to positively charged

Ru(bpy)$_3^{2+}$ (1.2 nm), resulting in the formation of high concentration of Ru(bpy)$_3^{2+}$ on the electrode surface. Thus, VMSF/CNNS/GCE electrode can enhance the ECL signal of Ru(bpy)$_3^{2+}$ while significantly reduce the amount of Ru(bpy)$_3^{2+}$ required, thereby lowering the cost of ECL detection.

3.2 Characterization of CNNS

The changes in surface groups of bulk g-C$_3$N$_4$ and CNNS before and after acid exfoliation were characterized by FT-IR technology, as shown in Fig. 2. The characteristic peaks in the range of 1200–1600 cm^{-1} and 810 cm^{-1} correspond to the stretching vibrations of CN heterocycles and the triazine ring, respectively. As shown, the spectra before and after acid exfoliation show no significant differences, indicating that the exfoliation process does not affect the skeleton of CN heterocycles. The absorption in the range of 3000–3500 cm^{-1} corresponds to the stretching vibrations of –NH$_2$ and –OH. It can be observed that the absorption peak of –OH stretching vibration in CNNS is significantly enhanced compared to that in bulk g-C$_3$N$_4$, indicating the introduction of a large number of OH groups during the acid treatment process. As is well known, GCE are primarily composed of sp^2 hybridized carbon. Thus, CNNS can be modified on the surface of GCE through π–π interactions. Simultaneously, the oxygen-containing groups in CNNS can form stable bonds with the silanol groups on VMSF through O–Si–O bonding, achieving a stable combination with VMSF. Fig. S1 (ESI)† shows the powder X-ray diffraction (XRD) characterization of g-C$_3$N$_4$ and CNNS. The two prominent diffractions at 13.0° and 27.4° correspond to the in-plane (100) and interlayer (002) diffractions of the graphite-like structure of carbon nitride, respectively.[56] CNNS exhibits a weak and broad interlayer (002) peak, attributed to its few-layer structure.[55] Additionally, the intensity of the peak at 13.0° becomes less pronounced, which may mainly result from the reduced stacking of carbon nitride layers and the partial disruption of in-plane repeating triazine units due to the sulfuric acid protonation process, potentially leading to more defects being embedded into the CNNS plane.[54] Scanning electron microscope (SEM) image also illustrate the layered structure of CNNS (Fig. S2, ESI†).

3.3 Characterization of VMSF/CNNS/GCE

The morphology and structure of VMSF were characterized by TEM. Fig. 3A presents a top-down view of VMSF in TEM. The image clearly shows the defect-free nanochannel membrane with uniform
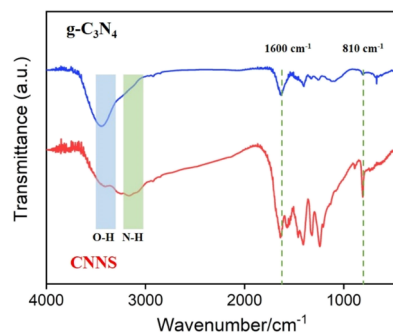

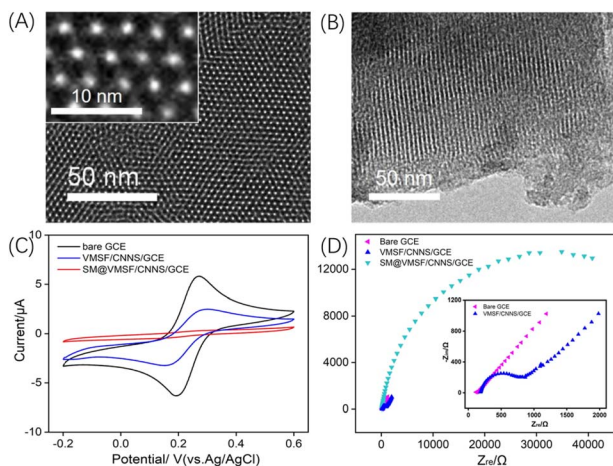Fig. 2 FTIR spectra of bulk g-C$_3$N$_4$ and CNNS.

Fig. 3 (A) Top-view TEM or HRTEM (inset) image of VMSF. (B) TEM image of cross-section of VMSF. CV (C) and EIS (D) plots of bare GCE, VMSF/CNNS/GCE and SM@VMSF/CNNS/GCE in 0.1 M KCl solution containing 2.5 mM Fe(CN)$_6^{3-/4-}$. The inset in is the magnified EIS plots of bare GCE and VMSF/CNNS/GCE (D).

Fig. 4 (A) The I_{ECL}−potential obtained on different electrodes in 10 μM Ru(bpy)$_3^{2+}$ and 15 mM Et$_3$N. (B) I_{ECL}−time curve obtained on VMSF/CNNS/GCE.

distribution. The inset of the high-resolution TEM (HRTEM) demonstrates a hexagonal arrangement of nanochannels, each with a diameter ranging from 2 to 3 nm. Fig. 3B displays a cross-sectional TEM image of VMSF, revealing the parallel nanochannel structure.

To further investigate the integrity of VMSF and the charge-selective permeability of the nanochannels, the electrochemical behaviour of Fe(CN)$_6^{3-/4-}$ was studied using cyclic voltammetry (CV) and electrochemical impedance spectroscopy (EIS) on different electrodes. As shown in Fig. 3C, almost no Faraday signal was observed on SM@VMSF/CNNS/GCE, only showing a charging current. This is attributed to the good integrity of the VMSF film, and the nanochannels being sealed by the micelles. After removing the micelles and obtaining open nanochannels, the signal of Fe(CN)$_6^{3-/4-}$ on VMSF/CNNS/GCE was suppressed compared to the bare GCE. This is due to the charge selectivity of VMSF nanochannels, which electrostatically repels Fe(CN)$_6^{3-/4-}$, thereby reducing the peak current. This result is further validated by EIS, as shown in Fig. 3D. The inset in Fig. 3D shows that bare GCE has minimal electron transfer resistance (R_{et}) due to its excellent electron transfer properties. When the nanochannels are sealed by micelles, the Fe(CN)$_6^{3-/4-}$ probe cannot reach the electrode surface, resulting in a significantly increased R_{et} for the SM@VMSF/CNNS/GCE electrode containing micelles. After removing the micelles and opening the channels, the negative charge of the channels, due to the ionization of silanol groups, repels the negatively charged Fe(CN)$_6^{3-/4-}$ probe, resulting in a slightly higher resistance for VMSF/CNNS/GCE compared to bare GCE. These results confirm the integrity of the VMSF film and the charge-selective permeability of the nanochannels.

3.4 Enhanced ECL on VMSF/CNNS/GCE

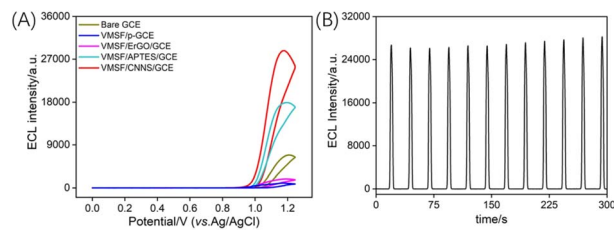Using GCE as the supporting electrode, CNNS, amino-modified siloxane (APTES), and electrochemically reduced graphene oxide (ErGO) were employed as modifying layers, or GCE was subjected to electrochemical polarization (p-GCE) to prepare the VMSF-modified electrodes. The ECL signals were compared among bare GCE, VMSF/CNNS/GCE, and VMSF/APTES/GCE in the Ru(bpy)$_3^{2+}$/Et$_3$N system. As shown in Fig. 4A, all electrodes exhibited oxidation starting at ∼1.0 V and a pronounced ECL signal at ∼1.2 V in the Ru(bpy)$_3^{2+}$/Et$_3$N solution. As shown in Fig. S3 (ESI),† during the anodic scan, Ru(bpy)$_3^{2+}$ is electrochemically oxidized into Ru(bpy)$_3^{3+}$, while Et$_3$N is oxidized to form the short-lived Et$_3$N radical cationic (Et$_3$N$^{•+}$), which further loses a proton to form the strongly reducing intermediate Et$_3$N$^•$. This radical can then reduce Ru(bpy)$_3^{3+}$ to Ru(bpy)$_3^{2+*}$, which returns to the ground state, emitting light (ECL signal). Compared to bare GCE, both VMSF/CNNS/GCE and VMSF/APTES/GCE showed significantly enhanced ECL signals. This is attributed to the electrostatic adsorption of negatively charged nanochannels on Ru(bpy)$_3^{2+}$, resulting in a substantial increase in the ECL signal. As a result, the concentration used is 10 μM, which is significantly lower than that is typically applied in common ECL sensing (more than 0.1 mM). The low concentration of ECL emitter reduced the cost of the proposed analysis.

However, the ECL signal value obtained on VMSF/APTES/GCE was only 55% of that on VMSF/CNNS/GCE. This is because APTES is a non-conductive organic adhesive layer that. Although APTES layer can achieve stable binding with VMSF but reduce the electroactive surface of GCE. The signals of VMSF/ErGO/GCE and VMSF/p-GCE also decreased compared to bare GCE, attributed to ErGO and the polarized GCE containing abundant phenolic hydroxyl groups. These groups are oxidized to form quinones during the positive potential scan, thereby quenching the ECL signal of Ru(bpy)$_3^{2+}$. Thus, the ECL signal of the VMSF-modified electrode obtained with CNNS as the adhesive and electrochemical layer was the highest. The stability of the prepared VMSF/CNNS/GCE electrode was examined by recording the ECL signal during continuous CV scans, as shown in Fig. 4B. The ECL intensity remained relatively stable during continuous scanning, indicating good stability.

3.5 Optimization of ECL detection conditions

As known, coreactant of Et$_3$N can significantly improve the ECL efficiency of the emitter Ru(bpy)$_3^{2+}$. At the same time, pH of the detection medium also affects the adsorption performance of

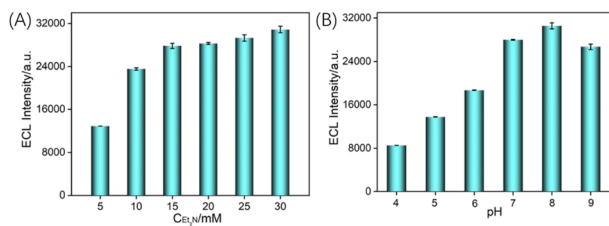Fig. 5 The relationship between ECL signal and (A) Et$_3$N concentration or (B) pH of the electrolyte.

nanochannels on Ru(bpy)$_3^{2+}$ and the deprotonation process of Et$_3$N. Thus, the effects of the co-reactant concentration and the pH of the electrolyte on the ECL signal were investigated. As shown in Fig. 5A, the ECL signal increased with the concentration of Et$_3$N and stabilized when the Et$_3$N concentration was 15 mM. Thus, 15 mM Et$_3$N was chosen for further experiments. The influence of pH values of the electrolyte on the ECL signal of the electrode was examined. As shown in Fig. 5B, the ECL intensity of Ru(bpy)$_3^{2+}$ significantly increases with increasing pH from 4 to 7, reaching a maximum at pH = 8. This is attributed to the increase in pH, leading to greater ionization of silanol groups as well as the increase in the negative charge density of the nanochannels, enhancing the electrostatic adsorption towards Ru(bpy)$_3^{2+}$ and further promoting the increase in ECL intensity. Meanwhile, with increasing pH, Et$_3$N$^{\bullet+}$ is more easily deprotonated to generate Et$_3$N$^{\bullet}$, which reacts with Ru(bpy)$_3^{3+}$ to produce more Ru(bpy)$_3^{2+*}$, contributing to signal amplification. However, when the pH increased from 8 to 9, the ECL signal decreased. This may be due to the reduced stability of the VMSF under alkaline conditions, which has a silica structure. Therefore, subsequent experiments were conducted using a solution with pH = 7.

3.6 ECL detection of TCP

Previous studies have indicated that phenolic compounds can quench the ECL signal of Ru(bpy)$_3^{2+}$. The possible mechanisms involve the intermediate radicals generated in the Ru(bpy)$_3^{2+}$/Et$_3$N reaction reacting with reducing molecules or resonance energy transfer occurring between quinone-like substances generated by the oxidation of phenols during anodic scanning and Ru(bpy)$_3^{2+*}$. Thus, a sensing system can be constructed to achieve the ECL detection of TCP based on the quenching effect of the ECL signal of Ru(bpy)$_3^{2+}$. Fig. 6A shows the ECL signals

obtained in the Ru(bpy)$_3^{2+}$/Et$_3$N solution at different concentrations of TCP. As observed, the ECL intensity decreases with increasing TCP concentration, indicating the quenching effect of TCP on the ECL signal of Ru(bpy)$_3^{2+}$. As shown in Fig. 6B, there is a good linear relationship between the ECL signal (I_{ECL}) and TCP concentration (C_{TCP}) in the range of 10 nM to 0.7 mM ($I_{\text{ECL}} = -39740 C_{\text{TCP}} + 26\,994$, $R^2 = 0.993$). The detection limit (DL) calculated based on a signal-to-noise ratio of three (S/N = 3) is 2.2 nM. Thus, the fabricated VMSF/CNNS/GCE exhibits high sensitivity and a low LOD for TCP detection, attributed to the significant electrostatic adsorption of the nanochannels on Ru(bpy)$_3^{2+}$.

3.7 Anti-fouling and anti-interference abilities of VMSF/CNNS/GCE

The anti-fouling and anti-interference abilities of VMSF/CNNS/GCE sensor were examined. Possible interferent (50 μM) was separately added to the Ru(bpy)$_3^{2+}$/Et$_3$N solution, including common pesticides such as diazinon, nitrobenzene, and carbendazim, or large molecule at a concentration of 50 μg mL^{-1}, including bovine serum albumin (BSA), dodecyl sodium sulfate (SDS), starch and lignin. The effect of analog of TCP, 2,4-dichlorophenol (DCP), has also been investigated. The ECL signals were measured in the presence of the above single interferent, or TCP (0.5 μM) (Fig. 7A). Even with significantly higher concentrations of the above substances compared to TCP, tested pesticides and large molecule showed no significant change. Due to its similar phenolic structure, DCP can quench ECL signals. However, the signal caused by DCP is significantly lower than that of TCP. This is because TCP has three chlorine atoms in its molecular structure, exhibiting a stronger electron-withdrawing effect and higher quenching the ECL signal of Ru(bpy)$_3^{2+}$. Since the detection mechanism relies on the quenching of the ECL of Ru(bpy)$_3^{2+}$ by phenolic substances, the presence of other phenolic contaminants might affect the detection. This issue can be addressed in two ways. Firstly, separation techniques such as chromatography or capillary electrophoresis can be employed to remove other phenolic interferents. Secondly, the linear extrapolation of the standard addition method can be used to determine the TCP concentration in real samples, eliminating the interference from phenolic contaminants in the matrix.
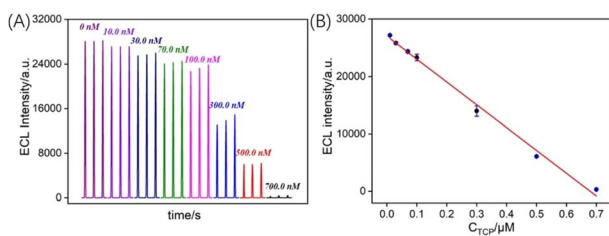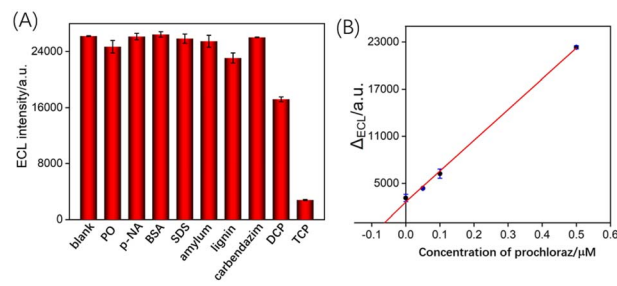

Fig. 6 (A) ECL signal obtained on VMSF/CNNS/GCE in presence of various concentrations of TCP. (B) The corresponding calibration curve.

Fig. 7 (A) ECL signal of Ru(bpy)$_3^{2+}$/Et$_3$N system measured on VMSF/CNNS/GCE sensor in presence of single substance or all substances simultaneously. (B) Linear relationship between ECL signal and TCP concentration in orange peel extract.

Sample	Added (μM)	Found^a (μM)	RSD (%)	Recovery (%, n = 3)
Pond water^b	0.05	0.049	1.0	98.0
	0.10	0.11	3.3	110.0
	0.50	0.53	3.0	106.0

^{a} The concentration was obtained after serum dilution. ^{b} The sample was diluted by a factor of 50.

3.8 ECL determination of TCP in real sample

To assess the capability of VMSF/CNNS/GCE in detecting TCP in real samples, the standard addition method was employed to determine the TCP content in pond water. Pond water, diluted 50 times with PBS, was used as the analytical sample, and the accuracy and precision of the method were validated. The results are presented in Table 1. As indicated, satisfactory recovery rates (98.0–110.0%) and small relative standard deviation (RSD) values (1.0–3.3%) were obtained. These findings suggest that the prepared sensor demonstrates good reliability and accuracy for TCP detection in real samples.

3.9 ECL detection of prochloraz in orange peel

Typically, the strategy for prochloraz detection involves adding pyridine hydrochloride salt to a mixture containing the target compound. Prochloraz and its metabolic intermediates are converted to TCP, and the prochloraz content is indirectly determined by measuring the TCP content. The metabolic process of Prochloraz is illustrated in Fig. S4 (ESI).† Initially, the imidazole ring of PCZ is cleaved, producing *N*-formyl-*N*-propyl-*N*-[2-(2,4,6-trichlorophenoxy)ethyl]urea (PCZ-FU) and *N*-propyl-*N*-[2-(2,4,6-trichlorophenoxy)ethyl]urea (PCZ-U). Subsequently, these two compounds further degrade into TCP.

Based on this mechanism, the developed sensor was also applied to detect prochloraz in orange peel extract as the matrix. As prochloraz was not detected in the sample, a standard solution of prochloraz at a concentration of 1.90 mg mL^{-1} was added to the orange peel extract. The conversion to TCP through heating and refluxing with pyridine hydrochloride salt was employed, and the original prochloraz content in the solution was determined through the extrapolation using the standard addition method (Fig. 7B). The concentration of prochloraz measured in the orange peel extract was 1.82 mg mL^{-1}, which is closely matched the added concentration, indicating the reliability in detecting prochloraz in real samples.

4. Conclusions

In this work, a method for the stable growth of VMSF on a GCE for the first time was introduced, utilizing conductive CNNS as a binding layer. The O–Si–O bond formed between CNNS and the nanochannels effectively stabilizes the growth of VMSF on the CNNS/GCE electrode. Compared to non-conductive molecular adhesives that passivate the electrode, CNNS exhibits good conductivity. Additionally, compared to ErGO, which contains abundant phenolic hydroxyl groups and quenches the ECL signal of Ru(bpy)$_3$$^{2+}$, CNNS does not significantly quench the ECL signal of Ru(bpy)$_3$$^{2+}$. Based on the electrostatic enrichment ability of VMSF for Ru(bpy)$_3$$^{2+}$, the fabricated VMSF/CNNS/GCE significantly enhances the ECL signal of Ru(bpy)$_3$$^{2+}$. Leveraging the quenching effect of phenols on the Ru(bpy)$_3$$^{2+}$/Et$_3$N system, VMSF/CNNS/GCE achieves sensitive detection of the environmental pollutant TCP. As the metabolic end product of prochloraz is TCP, prochloraz can be indirectly detected by measuring the TCP content. The constructed VMSF/CNNS/GCE demonstrates good sensitivity and low detection limit for ECL detection of TCP. Coupled with VMSF's resistance to fouling and interference, the fabricated VMSF-based sensor holds significant potential for direct and highly sensitive ECL detection in real samples.

Data availability

The data presented in this study are available on request from the corresponding author.

Conflicts of interest

There are no conflicts to declare.

Acknowledgements

References

1 R. Rodríguez, I. Boyer, G. Font and Y. Picó, *Analyst*, 2001, **126**, 2134–2138.
2 A. M. Vinggaard, U. Hass, M. Dalgaard, H. R. Andersen, E. V. A. Bonefeld-JØRgensen, S. Christiansen, P. Laier and M. E. Poulsen, *Int. J. Androl.*, 2006, **29**, 186–192.
3 H. Li, J. Li, C. Hou, S. Du, Y. Ren, Z. Yang, Q. Xu and X. Hu, *Talanta*, 2010, **83**, 591–595.
4 X. Zheng, S. Liu, X. Hua, F. Xia, D. Tian and C. Zhou, *Electrochim. Acta*, 2015, **167**, 372–378.
5 J. A. Buledi, A. R. Solangi, S. Q. Memon, S. I. Haider, S. Ameen, N. H. Khand, A. Bhatti and N. Qambrani, *Langmuir*, 2021, **37**, 3214–3222.
6 W. Zheng, R. Su, X. Lin and J. Liu, *Front. Chem.*, 2022, **10**, 954802.
7 C. Blasco, Y. Pico, J. Manes and G. Font, *J. Chromatogr. A*, 2002, **947**, 227–235.
8 Z. Liu, W. Qi and G. Xu, *Chem. Soc. Rev.*, 2015, **44**, 3117–3142.
9 W. Miao, *Chem. Rev.*, 2008, **108**, 2506–2553.
10 T. Zhang, J. Gong, Q. Han, W. Hu, F. Yan and J. Liu, *Talanta*, 2024, **277**, 126319.
11 J. Huang, T. Zhang, Y. Zheng and J. Liu, *Biosensors*, 2023, **13**, 317.

12 J. Gong, T. Zhang, T. Luo, X. Luo, F. Yan, W. Tang and J. Liu, *Biosens. Bioelectron.*, 2022, **215**, 114563.

13 J. Gong, T. Zhang, P. Chen, F. Yan and J. Liu, *Sens. Actuators, B*, 2022, **368**, 132086.

14 L. Li, Y. Chen and J.-J. Zhu, *Anal. Chem.*, 2017, **89**, 358–371.

15 X. Zhou, Y. Zou, H. Ru, F. Yan and J. Liu, *Anal. Chem.*, 2024, **96**, 10264–10273.

16 J. Huang, S. Xu, F. Yan and J. Liu, *Sens. Actuators, B*, 2024, **402**, 135119.

17 R. Yu, Y. Zhao and J. Liu, *Nanomaterials*, 2024, **14**, 390.

18 X. Zhou, X. Gu, S. Zhang, Y. Zou and F. Yan, *Microchem. J.*, 2024, **200**, 110315.

19 P. Zhou, L. Yao, K. Chen and B. Su, *Crit. Rev. Anal. Chem.*, 2019, **50**, 424–444.

20 J. Huang, X. Fan, F. Yan and J. Liu, *ACS Appl. Nano Mater.*, 2024, **7**, 7743–7752.

21 X. Deng, X. Lin, H. Zhou, J. Liu and H. Tang, *Nanomaterials*, 2023, **13**, 239.

22 J. Gong, H. Tang, M. Wang, X. Lin, K. Wang and J. Liu, *Mater. Des.*, 2022, **215**, 110506.

23 H. Zhou, G. Dong, A. Sailjoi and J. Liu, *Nanomaterials*, 2022, **12**, 65.

24 J. Xing, Q. Han, J. Liu and Z. Yan, *Front. Chem.*, 2023, **11**, 1324469.

25 D. Li, S. Xu, H. Jin, J. Wang and F. Yan, *Molecules*, 2023, **28**, 7515.

26 A. Walcarius, *Acc. Chem. Res.*, 2021, **54**, 3563–3575.

27 Y. Cui, S. Zhang, X. Zhou, F. Yan and W. Hu, *Microchem. J.*, 2023, **190**, 108632.

28 X. Ma, W. Liao, H. Zhou, Y. Tong, F. Yan, H. Tang and J. Liu, *J. Mater. Chem. B*, 2020, **8**, 10630–10636.

29 L. Zhou, H. Ding, F. Yan, W. Guo and B. Su, *Analyst*, 2018, **143**, 4756–4763.

30 A. Walcarius, *Curr. Opin. Electrochem.*, 2018, **10**, 88–97.

31 L. Yang, T. Zhang, H. Zhou, F. Yan and Y. Liu, *Front. Nutr.*, 2022, **9**, 987442.

32 X. Luo, T. Zhang, H. Tang and J. Liu, *Front. Nutr.*, 2022, **9**, 962736.

33 Y. Zhang, S. Zhang, J. Liu and D. Qin, *Molecules*, 2023, **28**, 6935.

34 Z. Yan, S. Zhang, J. Liu and J. Xing, *Molecules*, 2023, **28**, 5186.

35 Z. Zhou, W. Guo, L. Xu, Q. Yang and B. Su, *Anal. Chim. Acta*, 2015, **886**, 48–55.

36 Y. Zhou, X. Luo, F. Yan and Y. Mou, *ACS Omega*, 2023, **8**, 48491–48498.

37 C. Zhang, X. Zhou, F. Yan and J. Lin, *Molecules*, 2023, **28**, 6443.

38 H. Zhou, X. Ma, A. Sailjoi, Y. Zou, X. Lin, F. Yan, B. Su and J. Liu, *Sens. Actuators, B*, 2022, **353**, 131101.

39 F. Yan, X. Ma, Q. Jin, Y. Tong, H. Tang, X. Lin and J. Liu, *Microchim. Acta*, 2020, **187**, 470.

40 X. Ma, Z. Zhang, Y. Zheng and J. Liu, *Biosensors*, 2024, **14**, 403.

41 J. Huang, T. Zhang, G. Dong, S. Zhu, F. Yan and J. Liu, *Front. Chem.*, 2022, **10**, 900282.

42 F. Yan, M. Wang, Q. Jin, H. Zhou, L. Xie, H. Tang and J. Liu, *J. Electroanal. Chem.*, 2021, **881**, 114969.

43 S. Sayen and A. Walcarius, *Electrochem. Commun.*, 2003, **5**, 341–348.

44 F. Yan, T. Luo, Q. Jin, H. Zhou, A. Sailjoi, G. Dong, J. Liu and W. Tang, *J. Hazard. Mater.*, 2021, **410**, 124636.

45 F. Yan, J. Chen, Q. Jin, H. Zhou, A. Sailjoi, J. Liu and W. Tang, *J. Mater. Chem. C*, 2020, **8**, 7113–7119.

46 Q. Han, T. Zhang, M. Wang, F. Yan and J. Liu, *Molecules*, 2022, **27**, 8200.

47 Y. Zou, X. Zhou, L. Xie, H. Tang and F. Yan, *Front. Chem.*, 2022, **10**, 939510.

48 M. Wang, J. Lin, J. Gong, M. Ma, H. Tang, J. Liu and F. Yan, *RSC Adv.*, 2021, **11**, 9021–9028.

49 W. Chen, H. Ru, f. Yan and X. Mo, *RSC Adv.*, 2024, **14**, 18599.

50 Y. Zu and A. J. Bard, *Anal. Chem.*, 2000, **72**, 3223–3232.

51 Y. Qin, Z. Wang, J. Xu, F. Han, X. Zhao, D. Han, Y. Liu, Z. Kang and L. Niu, *Anal. Chem.*, 2020, **92**, 15352–15360.

52 W. J. Ong, L. L. Tan, Y. H. Ng, S. T. Yong and S. P. Chai, *Chem. Rev.*, 2016, **116**, 7159–7329.

53 S. C. Yan, Z. S. Li and Z. G. Zou, *Langmuir*, 2009, **25**, 10397–10401.

54 J. Wan, C. Pu, R. Wang, E. Liu, X. Du, X. Bai, J. Fan and X. Hu, *Int. J. Hydrogen Energy*, 2018, **43**, 7007–7019.

55 A. Walcarius, E. Sibottier, M. Etienne and J. Ghanbaja, *Nat. Mater.*, 2007, **6**, 602–608.

56 J. Qian, A. Yuan, C. Yao, J. Liu, B. Li, F. Xi and X. Dong, *ChemCatChem*, 2018, **10**, 4747–4754.